applied optics

Theoretical study on second-harmonic generation in two-dimensional nonlinear photonic crystals

Xiangnan Wang,[1,2] Xiaohui Zhao,[1,2] Yuanlin Zheng,[1,2] and Xianfeng Chen[1,2,*]

[1]State Key Laboratory of Advanced Optical Communication Systems and Networks, Department of Physics and Astronomy, Shanghai Jiao Tong University, Shanghai 200240, China
[2]Key Laboratory for Laser Plasma (Ministry of Education), Collaborative Innovation Center of IFSA (CICIFSA), Shanghai Jiao Tong University, Shanghai 200240, China
*Corresponding author: xfchen@sjtu.edu.cn

Received 3 November 2016; revised 20 December 2016; accepted 20 December 2016; posted 20 December 2016 (Doc. ID 280073); published 19 January 2017

We theoretically study second-harmonic generation in two-dimensional nonlinear photonic crystals and obtain a unified expression that combines nonlinear Raman–Nath diffraction, Čerenkov-type second-harmonic generation, and nonlinear Bragg diffraction. The analytical solution is deduced, and the theoretical result coincides well with the nonlinear Raman–Nath, nonlinear Čerenkov, and nonlinear Bragg diffraction phase-matching conditions. This method has potential applications in second-harmonic generation of more complicated two-dimensional and even three-dimensional nonlinear photonic crystals.

OCIS codes: (140.3490) Lasers, distributed-feedback; (060.2420) Fibers, polarization-maintaining; (060.3735) Fiber Bragg gratings; (060.2370) Fiber optics sensors.

https://doi.org/10.1364/AO.56.000750

1. INTRODUCTION

Quasi-phase-matched nonlinear frequency-conversion processes based on periodical domain reversed ferroelectric crystals have been widely investigated, such as second-harmonic generation (SHG), sum-frequency generation (SFG), difference-frequency generation (DFG), and so on. As special nonlinear interfaces, domain walls and nonlinear crystal boundaries have shown many strange features and nonlinear effects different from uniform bulk media in nonlinear frequency-conversion processes. In the vicinity of these nonlinear interfaces, enhanced nonlinear Čerenkov radiation can be observed, which arises from the lattice distortion or internal local electrical field. For example, a pair of symmetrically distributed Čerenkov second-harmonic generation (CSHG) dots could be generated when the fundamental wave (FW) propagates along the domain wall [1]. In the boundary of nonlinear crystals, CSHG dots could also be observed [1,2]. In addition, even enhanced CSHG could be obtained in the interface of two different nonlinear media [1]. Not limited to these special nonlinear interfaces, the most intensive studies about CSHG were on a variety of ferroelectric crystals. For example, CSHG could be generated in various one-dimensional (1D) nonlinear photonic crystals [2], and two-dimensional (2D) nonlinear photonic crystals such as rectangular, annular, decagonal, short-range ordered, and even random nonlinear photonic crystals [3–6]. In these ferroelectric crystals, CSHG, nonlinear Raman–Nath diffraction (NRND), and nonlinear Bragg diffraction (NBD) could be observed when the FW propagates along the transverse direction (perpendicular to traditional quasi-phase-matched (QPM) direction) of the crystal. As we know, nonlinear Čerenkov radiation is an autolongitudinal phase-matched process [1–7]. Different from nonlinear Čerenkov radiation, NRND is the SHG process that meets the transverse phase-matching condition [8–12], and it comes from the second-harmonic wave diffraction effect of different ferroelectric domains in ferroelectric crystals. As for NBD, it is a diffraction effect that meets both the transverse and longitudinal phase-matching conditions [11]. Compared with NRND and CSHG, NBD has a higher conversion efficiency because it meets the complete phase-matching condition. The NBD and multiple-order NRND has been observed and quantitatively analyzed in 1D photonic crystals [8,9,13]. In addition, NRND has been theoretically studied in rectangular [10] and annular [11,12] 2D nonlinear photonic crystals.

Although the theory of CSHG, NRND, and NBD in 1D nonlinear photonic crystals has been deeply discussed, the nonlinear process in 2D nonlinear photonic crystals has still rarely been investigated in theory. Theoretical studies in 2D photonic crystals merely stay at qualitative and incomplete analysis; for instance, NRND is determined by the transverse phase-matching condition. It is only a cursory and nonquantitative description of the SHG of 2D nonlinear photonic crystals.

Hence, how to obtain a uniform expression to describe the SHG, which combines NRND, CSHG, and NBD of 2D nonlinear photonic crystals, has become an urgent issue.

In this study, we start from the nonlinear coupled-wave equations [1,14], and then obtain a detailed analytical expression of the SHG of 2D nonlinear photonic crystals. The analytical result is a uniform expression, describing the nonlinear SHG, which combines NRND, CSHG, and NBD in 2D nonlinear photonic crystals. The SHG of several representative styles of 2D photonic crystals, including annularly, squarely, and hexagonally poled structures, was simulated, and the results were highly consistent with previous published experimental results in [3–5,10–12].

2. THEORETICAL MODEL AND ANALYSIS

We assume that the FW propagates along the z-axis, as shown in Fig. 1, and the periodic domain reverse pattern of the sample is a 2D distribution in the xy plane. If FW is a Gaussian beam and the modulation in the z-axis direction is neglected for simplicity, the dispersion function of amplitude will be written as $F(x,y)=e^{-\frac{x^2+y^2}{w^2}}$, where w is the beam waist. The amplitude of FW is assumed to be constant considering the high energy of the pump and low conversion efficiency of the nonlinear process. Considering the slowly varying envelope approximation, the coupled-wave equation [1,14] can be expressed as

$$\begin{cases} \frac{\partial A_1}{\partial z}=0 \\ \left(\frac{\partial}{\partial z}+\frac{i}{2k_2}\frac{\partial^2}{\partial x^2}+\frac{i}{2k_2}\frac{\partial^2}{\partial y^2}\right)A_2(z,x,y) \\ =-i\frac{2\pi k_2}{n_2^2}d_{\text{eff}}g(x,y)|A_1|^2F(x,y)^2e^{i(k_2-2k_1)z} \end{cases}, \tag{1}$$

where A_1 and $A_2(z,x,y)$ are the amplitudes of the FW and second-harmonic (SH) wave, respectively. d_{eff} is the effective second-order susceptibility. $F(x,y)=e^{-\frac{x^2+y^2}{w^2}}$ is the Gaussian distribution function of the FW, k_1 and k_2 are the wave vectors of the FW and SH, respectively. n_2 is the refractive index of the SH. $g(x,y)$ is the structure function of the nonlinear crystal. In periodically modulated nonlinear photonic crystals, $g(x,y)$ can be written as an expansion of Fourier series $g(x,y)=\sum_n\sum_m c_{nm}e^{-i(n\frac{2\pi}{\Lambda_x}x+m\frac{2\pi}{\Lambda_y}y)}$, where c_{nm} represent the Fourier coefficients. And finally, the SH intensity I_2 can be obtained as follows:

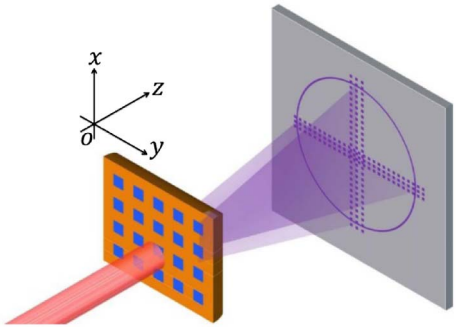

Fig. 1. Schematic illustration of SHG in a 2D nonlinear photonic structure.

$$\begin{aligned} I_2&=|A_2|^2 \\ &=\frac{4\pi^2k_2^2d_{\text{eff}}^2}{n_2^4}|A_1|^4z^2\left|\sum_n\sum_m c_{nm}F_1(k_x)F_2(k_y)\right|^2 \\ &\quad\times\operatorname{sinc}^2\left[\left(k_2-2k_1-\frac{k_x^2+k_y^2}{2k_2}\right)\frac{z}{2}\right], \end{aligned} \tag{2}$$

where

$$F_1(k_x)=\int_{-\infty}^{\infty}e^{-\frac{2x^2}{w^2}}e^{i\left(k_x-n\frac{2\pi}{\Lambda_x}\right)x}\mathrm{d}x=w\sqrt{\frac{\pi}{2}}e^{-\frac{w^2(k_x\Lambda_x-2n\pi)^2}{8\Lambda_x^2}}, \tag{3}$$

$$F_2(k_y)=\int_{-\infty}^{\infty}e^{-\frac{2y^2}{w^2}}e^{i\left(k_y-m\frac{2\pi}{\Lambda_y}\right)y}\mathrm{d}y=w\sqrt{\frac{\pi}{2}}e^{-\frac{w^2(k_y\Lambda_y-2m\pi)^2}{8\Lambda_y^2}}. \tag{4}$$

From Eqs. (2)–(4), I_2 is dominated by the factors $F_1(k_x)$, $F_2(k_y)$, and $\operatorname{sinc}^2[(k_2-2k_1-\frac{k_x^2+k_y^2}{2k_2})\frac{z}{2}]$. Obviously, the indexes of $F_1(k_x)$ and $F_2(k_y)$ are negative or zero. If the indexes are negative, I_2 will be strongly attenuated. Only if the indexes are all zeros will I_2 be enhanced. We should also note that, I_2 partly depends on the factor $\operatorname{sinc}^2[(k_2-2k_1-\frac{k_x^2+k_y^2}{2k_2})\frac{z}{2}]$, because it would reduce rapidly as $|k_2-2k_1-\frac{k_x^2+k_y^2}{2k_2}|$ increases. That is to say, I_2 is enhanced under the conditions $k_x\Lambda_x-2n\pi=0$ and $k_y\Lambda_y-2m\pi=0$ or $k_2-2k_1-\frac{k_x^2+k_y^2}{2k_2}=0$. The conditions of $k_x\Lambda_x-2n\pi=0$ and $k_y\Lambda_y-2m\pi=0$ are consistent with the transverse phase-matching conditions of NRND, so the factor $|\sum_n\sum_m c_{nm}F_1(k_x)F_2(k_y)|^2$ mainly describes NRND.

We assume k_{2z} is the z-component of k_2, so

$$k_{2z}=\sqrt{k_2^2-(k_x^2+k_y^2)}. \tag{5}$$

For $k_2^2\gg k_x^2+k_y^2$, the Taylor expansion of Eq. (5) can be expressed as

$$k_{2z}=k_2\sqrt{1-\frac{k_x^2+k_y^2}{k_2^2}}=k_2\left[1-\frac{k_x^2+k_y^2}{2k_2^2}-\frac{(k_x^2+k_y^2)^2}{8k_2^4}-\cdots\right]. \tag{6}$$

Ignoring higher-order terms in Eq. (6), then we obtain

$$k_{2z}=k_2\left(1-\frac{k_x^2+k_y^2}{2k_2^2}\right)=k_2-\frac{k_x^2+k_y^2}{2k_2}=2k_1. \tag{7}$$

Obviously, this is consistent with the autolongitudinal phase-matched condition of Čerenkov radiation [1,15]. Therefore the function $\operatorname{sinc}^2[(k_2-2k_1-\frac{k_x^2+k_y^2}{2k_2})\frac{z}{2}]$ plays a leading role in CSHG. The size of the CSHG radius $R_{\text{CSHG}}=\sqrt{k_x^2+k_y^2}=\sqrt{2k_2(k_2-2k_1)}$ only depends on the wavelength of the FW, because the values of k_1 and k_2 are uniquely determined by the Sellmeier equations [16].

3. SIMULATION AND RESULTS ANALYSIS

A. SH Intensity Simulation

The SHG of three specific examples of 2D nonlinear photonic crystals are simulated.

The structures of 2D nonlinear photonic crystals and the corresponding simulated SH patterns are shown in Fig. 2. For simplicity, lithium niobate crystal is used in our simulation. The annularly, squarely, and hexagonally poled structures are shown in Figs. 2(a), 2(c), and 2(e), respectively. The brown areas represent $g(x,y)=1$, and the blue areas represent $g(x,y)=-1$. The wavelength of FW $\lambda_1=0.8$ μm, and the wavelength of SH $\lambda_2=0.4$ μm. The beam waist of the input Gaussian beam is $w=50$ μm, and interaction distance is $z=1000$ μm. The type I ($oo-e$) phase-matching condition is used in our simulation. The refractive indices of the ordinary FW and extraordinary SH waves are $n_1=2.255$ and $n_2=2.331$, respectively [16]. The wave vectors of ordinary FW and extraordinary SH waves in the crystal are $k_1=17.713\ \mu m^{-1}$ and $k_2=36.615\ \mu m^{-1}$, respectively. These parameter values stay the same in all the following simulations.

In the annularly poled structure, a polar coordinate was used and the 2D annularly poled structure is only 1D periodical along the r direction. The modulated period $\Lambda_r=15$ μm, and the duty ratio $D_r=1/2$, then the Fourier coefficients and the factor $F(k_r)$ could be written as

$$\begin{cases} c_n=-\frac{i(e^{in\pi}-1)}{2n\pi} & n\neq 0 \\ c_n=0 & n=0 \end{cases}, \tag{8}$$

$$F(k_r)=w\sqrt{\frac{\pi}{2}}e^{-\frac{w^2(k_r\Lambda_r-2n\pi)^2}{8\Lambda_r^2}}=w\sqrt{\frac{\pi}{2}}e^{-\frac{w^2\left(\sqrt{k_x^2+k_y^2}\Lambda_r-2n\pi\right)^2}{8\Lambda_r^2}}. \tag{9}$$

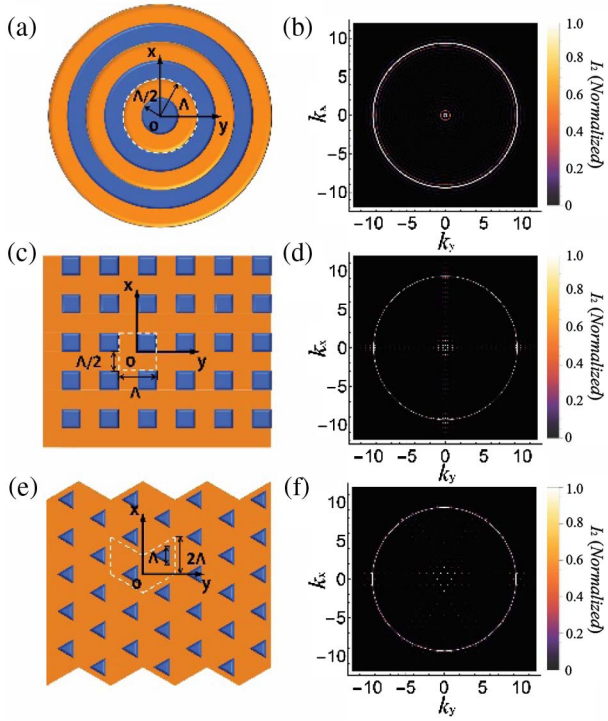

Fig. 2. Structures of 2D nonlinear photonic crystals and the corresponding simulated SH intensity. (a) Annularly poled structure; (c) squarely poled structure; (e) hexagonally poled structure. The white dotted line areas in (a), (c), and (e) represent the minimum 2D period areas. (b), (d), and (f) are the corresponding simulated SH intensity, respectively.

As shown in Fig. 2(b), in the circularly poled structure, the CSHG and the multiple-order NRND both display as rings. It is consistent with the experiment in [11,12]. NBD does not exist in this simulation, because the transverse and longitudinal phase-matching conditions are not satisfied simultaneously.

In the squarely poled structure, a rectangular coordinate was used, and $\Lambda_x=\Lambda_y=\Lambda=15$ μm; the duty ratio $D_x=1/2$ and $D_y=1/2$ are assumed. The Fourier coefficients, the factors $F_1(k_x)$ and $F_2(k_y)$ could be written, respectively, as

$$\begin{cases} c_{nm}=-\frac{e^{-i(2m+n)\pi}}{4mn\pi^2}(e^{im\pi}-1)(e^{in\pi}-1) & mn\neq 0 \\ \times(e^{im\pi}+e^{i2m\pi}+e^{i2(m+n)\pi}-e^{i(2m+n)\pi}) & \\ c_{nm}=\frac{i(e^{-im\pi}-1)}{2m\pi} & n=0,m\neq 0 \\ c_{nm}=\frac{i(e^{-in\pi}-1)}{2n\pi} & n\neq 0,m=0 \\ c_{nm}=\frac{1}{2} & n=0,m=0 \end{cases}, \tag{10}$$

$$F_1(k_x)=w\sqrt{\frac{\pi}{2}}e^{-\frac{w^2(k_x\Lambda_x-2n\pi)^2}{8\Lambda_x^2}}, \tag{11}$$

$$F_2(k_y)=w\sqrt{\frac{\pi}{2}}e^{-\frac{w^2(k_y\Lambda_y-2m\pi)^2}{8\Lambda_y^2}}. \tag{12}$$

As shown in Fig. 2(d), in the squarely poled structure, the CSHG displays as a ring, and the multiple-order NRND displays as square. The brightest areas of NRND are in four directions corresponding to $(1,0)$, $(0,1)$, $(-1,0)$, and $(0,-1)$, and it is consistent with the experiment in [4]. There are some bright points in the CSHG ring (NBD peaks), because their transverse and longitudinal phase-matching conditions are satisfied simultaneously.

In the hexagonally poled structure, $\Lambda_x=2\Lambda=8$ μm and $\Lambda_y=2\sqrt{3}\Lambda=8\sqrt{3}$ μm are assumed. The Fourier coefficients, the factors $F_1(k_x)$, $F_2(k_y)$ could be written, respectively, as

$$\begin{cases} c_{nm}=\frac{1}{4\pi^2}\left\{\begin{aligned}&\frac{2e^{-\frac{i}{6}(4m+3n)\pi}}{n(n+m)(n-m)}[1+e^{i(m+n)\pi}]\left[-2ne^{\frac{in\pi}{2}}\right.\\&+(n-m)e^{\frac{i(m+2n)\pi}{2}}+(n+m)e^{\frac{im\pi}{2}}\left.\right]\\&-\frac{e^{-i(m+n)\pi}}{n(n+m)(n-m)}(-1+e^{i2n\pi})[-2ne^{im\pi}\\&+(n-m)e^{i(2m+n)\pi}+(n+m)e^{in\pi}]\end{aligned}\right\} & n\neq 0,m^2\neq n^2 \\ c_{nm}=\frac{e^{-\frac{2i}{3}(4m+3n)\pi}}{2m^2\pi^2}(1+e^{im\pi})\left[2+e^{\frac{im\pi}{2}}(im\pi-2)\right. & \\ \left.+2m\pi\sin(m\pi)\right] & n=0,m\neq 0 \\ c_{nm}=\frac{e^{-in\pi}}{8n^2\pi^2}\left[2e^{\frac{in\pi}{3}}(1+e^{i2n\pi})(e^{in\pi}-1-in\pi)\right. & \\ \left.-(e^{i2n\pi}-1)(e^{i2n\pi}-1+i2n\pi)\right] & n\neq 0,n=m \\ c_{nm}=\frac{e^{-in\pi}}{8n^2\pi^2}\left[4e^{\frac{i2n\pi}{3}}-1-e^{i4n\pi}+i2n\pi\right. & \\ \left.+e^{i2n\pi}(2-i2n\pi)+e^{\frac{i5n\pi}{3}}(-4+i4n\pi)\right] & n\neq 0,n=-m \\ c_{nm}=\frac{3}{4} & n=m=0 \end{cases}, \tag{13}$$

$$F_1(k_x) = w\sqrt{\frac{\pi}{2}}e^{-\frac{w^2(k_x\Lambda_x-2n\pi)^2}{8\Lambda_x^2}} = w\sqrt{\frac{\pi}{2}}e^{-\frac{w^2(k_x\Lambda-n\pi)^2}{8\Lambda^2}}, \quad (14)$$

$$F_2(k_y) = w\sqrt{\frac{\pi}{2}}e^{-\frac{w^2(k_y\Lambda_y-2m\pi)^2}{8\Lambda_y^2}} = w\sqrt{\frac{\pi}{2}}e^{-\frac{w^2\left(3k_y\Lambda-\sqrt{3}m\pi\right)^2}{72\Lambda^2}}. \quad (15)$$

As shown in Fig. 2(f), in the hexagonally poled structure, the CSHG displays as a ring, and the multiple-order NRND displays as hexagonal. The brightest areas of NRND are in six directions corresponding to (1, 0), $(\sqrt{3}/2, 1/2)$, $(-\sqrt{3}/2, 1/2)$, $(-1, 0)$, $(-\sqrt{3}/2, -1/2)$, and $(\sqrt{3}/2, -1/2)$, and it is consistent with the experiment in [17]. There are also some intensive NBD peaks in the CSHG ring, the same as the case of the squarely poled structure.

In previous research, the analysis of the CSHG intensity was incomplete, such as $I_{\mathrm{CSHG}} \propto z^2\,\mathrm{sinc}^2[(k_2 - 2k_1 - \frac{k_x^2+k_y^2}{2k_2})\frac{z}{2}]$ [4], and it did not take into account the contribution of the factor $|\sum_n\sum_m c_{nm}F_1(k_x)F_2(k_y)|^2$. From Eqs. (2)–(4), one can see that the NRND and CSHG intensities are affected by each other. The values of $|\sum_n\sum_m c_{nm}F_1(k_x)F_2(k_y)|^2$ and $\mathrm{sinc}^2[(k_2 - 2k_1 - \frac{k_x^2+k_y^2}{2k_2})\frac{z}{2}]$ dominate the change of I_2 simultaneously. Thus the intensity of the CSHG ring is not constant.

B. Dependence of SHG Intensity on the Duty Ratio

Next, we specifically analyze the SHG in a squarely poled structure. From Eqs. (2) and (10), it is obvious that the (n, m)-order NRND intensity is proportional to $|c_{nm}|^2$. However, there is no nonzero even-order NRND in the condition of $D_x = D_y = D = 1/2$, because $|c_{nm}|^2$ equal to zeros for n or m is a nonzero even number. That is to say, the multiorder NRND intensities are affected by the duty ratio. Therefore, we simulate the nonzero even-order and odd-order NRND intensities, respectively, by changing the duty ratio. $D_x = D_y = D$ is assumed for simplicity, and the Fourier coefficients are obtained in Eq. (13). As shown in Fig. (3), we display the (1, 11)-order and (1, 12)-order NRND SH intensities depending on the duty ratio. One can see that both the even- and odd-order NRND intensities equal to zeros for $D = 0$ or $D = 1$, because it means no periodical reversed domains. In addition, the (1, 11)-order NRND intensity reaches the maximal value, and the (1, 12)-order NRND intensity reaches the minimum value for $D = 1/2$

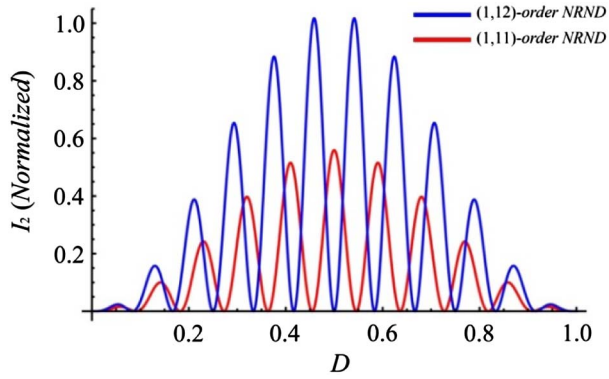

Fig. 3. Even order and odd order NRND SH intensity depending on the duty ratio. The red line represents (1, 11)-order NRND, and the blue line represents the (1, 12)-order NRND.

C. Generation of NBD

In Fig. 2(d), one can see that the NRND intensity is enhanced near R_{CSHG}. This phenomenon can be treated as the resonance effect of NRND and CSHG [18]. When the transverse and longitudinal phase-matching conditions are exactly satisfied at the same time, the NBD will be generated [11]. In order to generate the high-efficiency NBD, we can change the modulated period to an appropriate value. For example, as shown in Fig. 4, the bright NBD ring in the circularly poled structure is obtained by changing the value of the modulated period to $\Lambda_r = 14.1379$ μm, which is derived from the equation $R_{\mathrm{CSHG}} = \sqrt{2k_2(k_2 - 2k_1)} = \sqrt{(2n\pi/\Lambda_r)^2}$.

D. Dependence of SHG Intensity on the Incident Polarization Angle

In fact, the effective nonlinear coefficient d_{eff} in Eq. (1) depends on the incident polarization angle of FW. In lithium niobate crystal, $d_{\mathrm{eff}} = d_{31}\sin\theta - d_{22}\cos\theta\sin 3\varphi$ for type I phase-matching conditions, where θ is the incident angle of FW vector corresponding to the z-axis, and φ is the FW azimuth in the xy plane. In our simulation, FW is incident along the z-axis, so $\theta = 0$, $d_{\mathrm{eff}} = -d_{22}\sin 3\varphi$. Thus we can obtain the SHG intensity for different incident polarization angles of the FW as follows:

$$I_2 = \frac{4\pi^2k_2^2d_{22}^2}{n_2^4}\sin^2 3\varphi|A_1|^4z^2\left|\sum_n\sum_m c_{nm}F_1(k_x)F_2(k_y)\right|^2 \times \mathrm{sinc}^2\left[\left(k_2 - 2k_1 - \frac{k_x^2+k_y^2}{2k_2}\right)\frac{z}{2}\right]. \quad (17)$$

$$\begin{cases} c_{nm} = \frac{e^{-i2m\pi}}{4mn\pi^2}[(-2e^{i2m\pi} + e^{i2Dm\pi} + e^{i2(1+D)m\pi})(e^{i2Dn\pi} - 1) - 4e^{i[m+2Dm+(D-1)n]\pi} \times \sin m\pi\sin(D-1)n\pi] & mn \neq 0 \\ c_{nm} = \frac{i}{2m\pi}[-2D + e^{2i(-1+D)m\pi} + (-1+2D)e^{i2Dm\pi}] & n = 0, m \neq 0 \\ c_{nm} = \frac{i}{2n\pi}[-2D + e^{2i(-1+D)n\pi} + (-1+2D)e^{i2Dn\pi}] & n \neq 0, m = 0 \\ c_{nm} = 1 - 2D^2 & n = 0, m = 0 \end{cases} \quad (16)$$

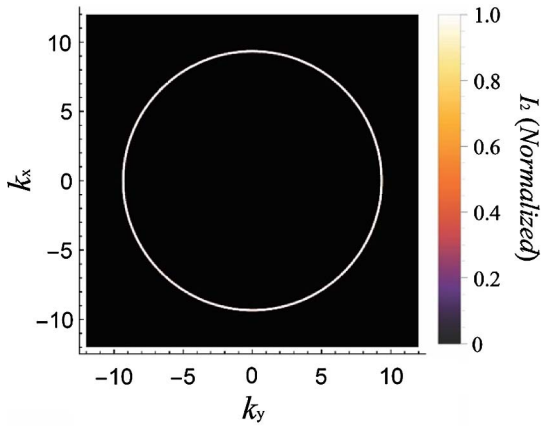

Fig. 4. NBD in the circularly poled structure for $\Lambda_r = 14.1379$ μm and $n = 21$.

Inspired by the analytical results, we can obtain the SH intensity distribution in all the incident polarization angles and more 2D nonlinear photonic crystals. One can also design the pattern of 2D nonlinear photonic crystals to realize any SH distribution.

4. CONCLUSIONS

In summary, we theoretically studied the SHG of 2D nonlinear photonic crystals and obtained a uniform expression that combines NRND, CSHG, and NBD. Annularly, squarely, and hexagonally poled structures are calculated. The nonlinear Čerenkov radiation rings and multiple-order Raman–Nath diffraction peaks could be observed in the simulated results. The results not only agree well with the nonlinear Čerenkov and nonlinear Raman–Nath phase-matching conditions, but also correspond with the experiment phenomenon. What is more, we also obtain the NBD generation by changing the polarized period to an appropriate value. The theoretical method used in this work provides an effective way to study nonlinear CSHG and NRND at the same time. In addition, this method has potential applications in SHG of 2D and even three-dimensional nonlinear photonic crystals, which involves more complicated modulation on the nonlinear susceptibility.

Funding. National Natural Science Foundation of China (NSFC) (61235009).

REFERENCES

1. Y. Sheng, V. Roppo, K. Kalinowski, and W. Krolikowski, "Role of a localized modulation of $\chi^{(2)}$ in Čerenkov second-harmonic generation in nonlinear bulk medium," Opt. Lett. **37**, 3864–3866 (2012).
2. V. Roppo, K. Kalinowski, Y. Sheng, W. Krolikowski, C. Cojocaru, and J. Trull, "Unified approach to Čerenkov second harmonic generation," Opt. Express **21**, 25715–25726 (2013).
3. L. Mateos, P. Molina, J. Galisteo, C. Lopez, L. E. Bausa, and M. O. Ramirez, "Simultaneous generation of second to fifth harmonic conical beams in a two dimensional nonlinear photonic crystal," Opt. Express **20**, 29940–29948 (2012).
4. S. M. Saltiel, Y. Sheng, N. Voloch-Bloch, D. N. Neshev, W. Krolikowski, A. Arie, K. Koynov, and Y. S. Kivshar, "Cerenkov-type second-harmonic generation in two-dimensional nonlinear photonic structures," IEEE J. Quantum Electron. **45**, 1465–1472 (2009).
5. Y. Sheng, V. Roppo, Q. Kong, K. Kalinowski, Q. Wang, C. Cojocaru, J. Trull, and W. Krolikowski, "Tailoring Čerenkov second-harmonic generation in bulk nonlinear photonic crystal," Opt. Lett. **36**, 2593–2595 (2011).
6. M. Ayoub, P. Roedig, K. Koynov, J. Imbrock, and C. Denz, "Čerenkov-type second-harmonic spectroscopy in random nonlinear photonic structures," Opt. Express **21**, 8220–8230 (2013).
7. A. Fragemann, V. Pasiskevicius, and F. Laurell, "Second-order nonlinearities in the domain walls of periodically poled $KTiOPO_4$," Appl. Phys. Lett. **85**, 375–377 (2004).
8. Y. Sheng, Q. Kong, W. J. Wang, K. Kalinowski, and W. Krolikowski, "Theoretical investigations of nonlinear Raman–Nath diffraction in the frequency doubling process," J. Phys. B **45**, 055401 (2012).
9. A. M. Vyunishev, V. V. Slabko, I. S. Baturin, A. R. Akhmatkhanov, and V. Y. Shur, "Nonlinear Raman–Nath diffraction of femtosecond laser pulses," Opt. Lett. **39**, 4231–4234 (2014).
10. A. M. Vyunishev and A. S. Chirkin, "Multiple quasi-phase-matching in nonlinear Raman–Nath diffraction," Opt. Lett. **40**, 1314–1317 (2015).
11. S. M. Saltiel, D. N. Neshev, R. Fischer, W. Krolikowski, A. Arie, and Y. S. Kivshar, "Generation of second-harmonic conical waves via nonlinear Bragg diffraction," Phys. Rev. Lett. **100**, 103902 (2008).
12. S. M. Saltiel, D. N. Neshev, R. Fischer, W. Krolikowski, A. Arie, and Y. S. Kivshar, "Generation of second-harmonic Bessel beams by transverse phase-matching in annular periodically poled structures," Jpn. J. Appl. Phys. **47**, 6777–6783 (2008).
13. S. M. Saltiel, D. N. Neshev, W. Krolikowski, A. Arie, O. Bang, and Y. S. Kivshar, "Multiorder nonlinear diffraction in frequency doubling processes," Opt. Lett. **34**, 848–850 (2009).
14. Y. Sheng, Q. Kong, V. Roppo, K. Kalinowski, Q. Wang, C. Cojocaru, and W. Krolikowski, "Theoretical study of Čerenkov-type second-harmonic generation in periodically poled ferroelectric crystals," J. Opt. Soc. Am. B **29**, 312–318 (2012).
15. Y.-Y. Yue, H. Xiao, B. Yang, R.-E. Lu, X.-H. Hong, C. Zhang, Y.-Q. Qin, and Y.-Y. Zhu, "Theoretical study on the Cerenkov-type second-harmonic generation in optical superlattices without paraxial approximation," Opt. Express **24**, 1539–1545 (2016).
16. G. J. Edwards and M. Lawrence, "A temperature-dependent dispersion equation for congruently grown lithium niobate," Opt. Quantum Electron. **16**, 373–375 (1984).
17. Y. Zhang, F. Wang, K. Geren, S. N. Zhu, and M. Xiao, "Second-harmonic imaging from a modulated domain structure," Opt. Lett. **35**, 178–180 (2010).
18. K. Kalinowski, P. Roedig, Y. Sheng, M. Ayoub, J. Imbrock, C. Denz, and W. Krolikowski, "Enhanced Čerenkov second-harmonic emission in nonlinear photonic structures," Opt. Lett. **37**, 1832–1834 (2012).